THE ASTROPHYSICAL JOURNAL, 468:739–748, 1996 September 10

PHOTOEVAPORATED FLOWS FROM H II REGIONS

SUSANA LIZANO,[1] JORGE CANTÓ,[1] GUIDO GARAY,[2] AND DAVID HOLLENBACH[3]
Received 1995 December 4; accepted 1996 March 14

ABSTRACT

We model the dynamics of a fast, isothermal ionized stellar wind loaded with mass injected from photoevaporated globules surrounding the massive star. The effect of the mass injection is to produce a density profile such that the ionization front can be trapped for 10^5 yr, depending on the physical characteristics of the neutral globules inside the H II region.

We find that for neutral globules with sizes $R_g \sim 0.01$ pc, masses of $M_g \sim 1\ M_\odot$, and number densities $N_g \sim 2 \times 10^4$ pc^{-3}, thought to be representative of globules in regions of massive star formation, the implied mean density and size of the mass-loaded regions of ionized gas are about 10^3–10^4 cm^{-3} and about 0.1 pc, respectively, similar to those of compact H II regions. Dust absorption of ionizing photons is important and decreases the densities of the mass-loaded winds with respect to their dust-free counterparts. Also, mass-loaded winds with dust evolve more slowly, since the dusty globules survive for longer times than the dust-free ones.

Our models predict ionized flows with mass flow rates of $\dot{M} \sim 10^{-5}$ to $10^{-4}\ M_\odot$ yr^{-1}. These ionized flows could be studied in radio recombination lines. Assuming N_g does not decline sharply with distance to the central star, the ionized flow will recombine after the characteristic "Strömgren" radius r_S at which the ionizing photon rate goes to zero. Therefore, after this radius a neutral flow will accelerate adiabatically to a terminal velocity of $v_{\rm H\,I} \sim 40$ km s^{-1}. Neutral flows of this type could be searched for in the neutral hydrogen line at 21 cm in absorption against the continuum of the compact H II regions.

Subject headings: H II regions — ISM: globules — ISM: jets and outflows — radio lines: ISM

1. INTRODUCTION

Compact H II regions are thought to be produced by recently formed O and early B type stars still embedded in their parent cloud. They are usually found in groups and are characterized by having electron densities in the range of approximately 10^3–10^4 cm^{-3}, sizes 0.05–0.3 pc, and emission measures approximately 10^7 pc cm^{-6} (e.g., Wood & Churchwell 1989, hereafter WC; Garay et al. 1993 hereafter GRMC; Kurtz, Churchwell, & Wood 1994, hereafter KCW). Since regions of ionized gas born in a medium of constant density are expected to expand into the lower pressure ambient neutral gas, then their sizes would indicate their ages. For instance, using the classical model of the evolution of H II regions (e.g., Spitzer 1978), a region of ionized gas excited by an O7 star, born in a medium with an ambient density of 10^5 cm^{-3}, would have expanded to a radius of 0.1 pc in a lapse of time of about 10^4 years. The small sizes of the compact H II regions ($\sim$0.1 pc) would then imply that they are very young objects, with lifetimes of about 10^4 yr. In an ambient medium with a density gradient, the evolution of the H II regions can be even faster (e.g., Franco, Tenorio-Tagle, & Bodenheimer 1989, 1990), implying that the compact regions could be even younger. WC found, however, that there are too many compact and ultracompact (hereafter UC; diameters <0.05 pc) H II regions to be consistent with their short dynamical ages. They concluded that the expansion of these H II regions is inhibited by some mechanism, so that their small sizes do not necessarily indicate that they are extremely young. Several suggestions have been made to explain the large discrepancy between the observed number of compact and UC H II regions and the number expected from the formation rate of massive stars and the time they spend in this compact phase (see Churchwell 1990).

Van Buren et al. (1990) and Mac Low et al. (1991) propose that compact H II regions are excited by O stars that are in motion relative to the molecular cloud and that have formed a bow shock supported by its stellar wind. In this model, the ram pressure of the molecular gas flowing into the shock of a moving H II region balances the pressure that the stellar wind exerts on the ionized gas producing static cometary configurations, neither expanding nor contracting. H II regions would then remain compact as long as the moving star remains embedded within the dense core of the molecular cloud.

Alternatively, Hollenbach et al. (1994) propose that newly formed OB stars are surrounded by massive primordial disks which provide the source for the dense ultracompact regions of ionized gas. The dense gas that is photoevaporated from the circumstellar disk around the star gives rise to a UC H II region. The reservoir of dense gas within the disks may last for a period of about 10^5 yr. Thus, these types of UC H II regions could live much longer than their estimated "dynamical age" because they are constantly being replenished by a dense circumstellar reservoir.

These two models, however, may not explain fully the apparent paradox between the large number of compact H II regions and their short dynamical ages. Of the large sample of compact H II regions surveyed by WC and KCW, only 20% exhibit cometary morphologies. In addition, investigations of the kinematics of cometary-like H II regions using radio recombination lines (Wood & Churchwell 1991; Garay, Lizano, & Gómez 1994) show that cometary morphologies are produced both by bow shock flows as well as by champagne flows (Tenorio-Tagle 1979; Yorke, Tenorio-Tagle, & Bodenheimer 1983; Franco et al. 1990).

[1] Instituto de Astronomía, UNAM, Apdo. Postal 70-264, 04510 México, D.F., México.
[2] Departamento de Astronomía, Universidad de Chile, Casilla 36-D, Santiago, Chile.
[3] Nasa Ames Research Center, MS 245-3, Moffett Field, CA 94035.

On the other hand, firm evidence for the presence of photoevaporated disks is available in only one case, the ultracompact H II region around MWC 349A (see, e.g., Planesas, Martín-Pintado, & Serabyn 1992; Thum, Martín-Pintado, & Bachiller 1992; Rodríguez & Bastian 1994), although the large fraction of the presently detected compact H II regions that remain unresolved are potential candidates.

Recently, DePree, Rodríquez, & Goss (1995) proposed that UC H II regions are born in very high density ($n > 10^7$ cm^{-3}) and warm ($T_K \sim 100$ K) molecular cores, thus arriving to their final equilibrium radius (e.g., Dyson & Williams 1980) in short timescales of about 10^4 yr. This possibility is supported by the detection, with single dish instruments, of very dense molecular material in regions of high-mass star formation (e.g., Cesaroni, Walmsley, & Churchwell 1992; Olmi, Cesaroni, & Walmsley 1993), but it has to be confirmed with high spatial resolution VLA detection of dense cores around UC H II regions (e.g., Garay & Rodríguez 1990; Garay, Moran, & Rodríguez 1993; Cesaroni et al. 1994). An interesting work along these lines is that of Hofner et al. (1996), who studied the G9.62+0.20 star-forming region with the Owens Valley interferometer and found UC H II regions of different ages immersed in high-density molecular gas.

Here we present yet an alternative model that lengthens the compact phase of H II regions and reconciles their observed small sizes with their long lifetimes. This model should be particularly appropriate for compact H II regions with irregular morphologies, which make up about 20% of the H II regions in the samples of WC and KCW. The model we propose in this paper is that of an H II region formed in a primordial clumpy medium, which we will show can result in long-lived ($\sim 10^5$ yr) compact H II regions. The presence of externally ionized globules near recently formed stars has been reported in several works (e.g., Lacques & Vidal 1979; Felli, Hjellming, & Cesaroni 1987; Garay, Moran, & Reid 1987; Churchwell et al. 1987; Garay 1987; Felli et al. 1993). Their spectra have also been modeled by Pastor, Cantó, & Rodríguez (1991). The globules could be the result of a fragmentation process during the gravitational collapse of a cloud core that led to formation of a massive star. They may represent cores about to undergo, or in the process of, collapse to form a low-mass star.

The dynamics of photoevaporation globules have been studied theoretically by Oort & Spitzer (1955), Dyson (1968, 1973), Kahn (1969), Tenorio-Tagle (1977), Bedjin & Tenorio-Tagle (1984), Bertoldi (1989), and Bertoldi & McKee (1990). Here we study the mass injection due to the photoevaporation of neutral globules inside regions of ionized gas (Dyson 1994) and how this injection lengthens the compact phase of H II regions. In particular, since OB stars are known to have very powerful winds, we model a fast ($v_w > 2000$ km s^{-1} initially) isothermal stellar wind loaded with mass from these globules, in the same way as Hartquist et al. (1986) considered the mass loading due to hydrodynamical ablation of pressure confined globules inside windblown bubbles: bow shocks will exist around the globules in which the injected material is accelerated up to the wind speed. In this work, we do not consider the hydrodynamical ablation process, which is expected to be smaller than the mass loss due to the photoevaporation of globules exposed to the high ionizing photon rates characteristics of massive stars. Recent calculations show that, under the conditions appropriate for young massive stars, mass loading due to the hydrodynamical ablation of self-gravitating clumps is less important than that due to photoevaporation (Arthur & Lizano 1996). This happens because ablation of self-gravitating globules occurs only through mixing layers which have a low ablation rate compared with the photoevaporation rate of globules exposed to high ionizing photon fluxes. In the present work, it is shown that photoevaporation alone can inject sufficient mass into the outflow to absorb the ionizing photon flux (i.e., form a quasi-stationary and finite Strömgren radius) and produce compact H II regions for at least 10^5 yr. We include the effect of dust absorption of ionizing photons in the mean flow and in the mass injection from the neutral globules. Outside the Strömgren radius, the flow becomes neutral. The neutral flow will adiabatically accelerate to about 40 km s^{-1} with a mass flow rate of 10^{-5} to $10^{-4}\,M_\odot$ yr^{-1}.

Recently, Dyson, Williams, & Redman (1995) and Redman, Williams, & Dyson (1996) have studied models of mass injection in H II regions. The difference with respect to this work is that in their models the mass injection rate is a free function, while in our models we calculate the mass injection rate corresponding to the photoevaporation of globules in the ionizing photon flux of a given central star and the time evolution of this mass injection rate as the globules are destroyed.

2. MODEL

2.1. *Overall Characteristics*

We model a fast, isothermal, ionized stellar wind that is loaded with mass due to the photoevaporation of neutral globules (see Fig. 1). The model is based on observations by GRMC of regions of ionized gas covering a fivefold range in angular resolution. These observations suggested that several of the UC H II regions cataloged by WC may not be internally excited but correspond to the ionized surfaces of very dense neutral structures embedded within inhomogeneous regions of ionized gas excited by a single luminous

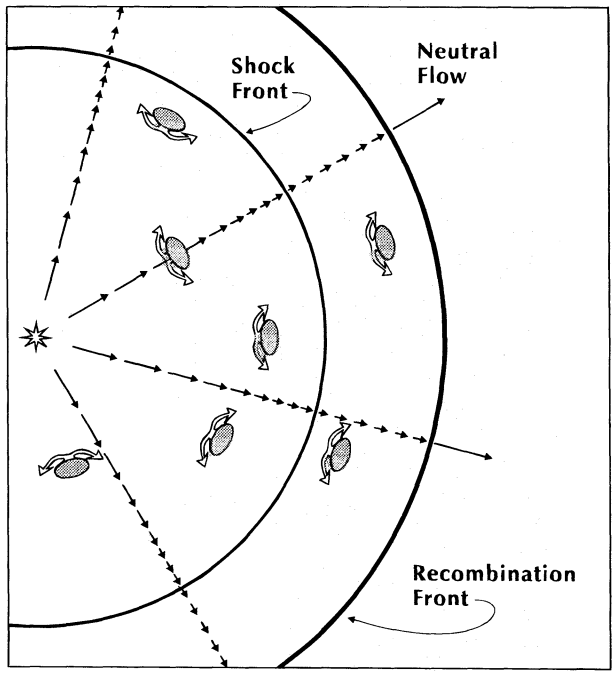

FIG. 1.—Cartoon of a wind mass loaded by the photoevaporation of neutral globules.

star. These partially ionized neutral globules are the so-called PIGs. In our model, the PIGs would provide a source of dense ionized plasma near the star that can trap the ionization front or produce a core-halo morphology for timescales of about 10^5 yr, depending on the distribution of neutral globules. In fact, from the contour maps of several irregular H II regions in the surveys of WC and KCW (e.g., G35.05−0.52, G111.28−0.66, and G31.28+0.06), one derives a number density of globules between 2×10^3 and 3×10^4 pc^{-3}, globule radius between 0.006 and 0.02 pc, and volume filling factors between 0.006 and 0.06. The globules have, typically, radii $R_g \sim 0.01$ pc, which we adopt as the standard radius. As a standard value for the number density of PIGs, we adopt $N_g \sim 2 \times 10^4$ pc^{-3}, consistent with the values quoted above and the density of PIGs observed in the Orion Nebula region (e.g., Garay 1987). We assume that the mass of an individual globule is about 1 $M_\odot$, implying that the turbulent or thermal velocities in the globule would be of order 1 km s^{-1}, if in virial equilibrium. This mass implies a hydrogen number density within the globule of about 4×10^6 cm^{-3}. Hereafter we will refer to globules with these properties as the standard globules. Finally, we consider central stars with Lyman-continuum photon luminosities in the range 10^{47}–10^{49} photons s^{-1}, corresponding to zero-age main sequence (ZAMS) stars of spectral types between B0 and O6.

2.2. *Equations*

We assume that the wind density is sufficiently high that it does not have an adiabatic phase (e.g., Weaver et al. 1977). Under these assumptions, the steady state equations in spherical coordinates for the gas are as follows:

1. The equation of continuity,

$$\frac{1}{r^2}\frac{d(r^2\rho v)}{dr} = \dot{q}\,, \tag{1}$$

where r is the distance to the cental star, v is the gas velocity, ρ is the ionized gas density, and $\dot{q}$ is a mass source term (g cm^{-3} s^{-1}), which will be discussed below;

2. The momentum equation,

$$\rho v\frac{dv}{dr} = -c_i^2\frac{d\rho}{dr} - (v + v_{\rm inj})\dot{q}\,, \tag{2}$$

where c_i is the isothermal sound speed of the ionized gas and $v_{\rm inj}$ is the injection velocity of the photoevaporated material, which has a direction opposite to the flow speed. As discussed below, $v_{\rm inj}$ has the magnitude of c_i; therefore, it becomes an important effect in the region in which the flow speed $v \leq c_i$.

3. The ionizing photon rate equation,

$$\frac{d\dot{S}}{dr} = -\dot{S}A_g N_g - 4\pi r^2\alpha_R\left(\frac{\rho}{m_{\rm H}}\right)^2 - \sigma_d n_{inj}\dot{S}\,, \tag{3}$$

where $\dot{S}$ is the total number of ionizing photons ($h\nu > 13.6$ eV) flowing through a shell of radius r per unit time, A_g and N_g are the area and number density of the globules, respectively, α_R is the case B recombination rate to the energy levels $n > 1$, $m_{\rm H}$ is the proton mass, $\sigma_d = 2 \times 10^{-21}$ cm^2 is the dust UV mean cross section per hydrogen atom and $n_{\rm inj}$ is the hydrogen number density of the material injected by the photoevaporated globules into the flow. Since the total mass density is $\rho = m_{\rm H}(n_w + n_{\rm inj})$, where n_w is the density of the stellar wind, then

$$n_{\rm inj} = \frac{\dot{M}_w}{4\pi r^2 v m_{\rm H}}\left(\frac{\dot{M}}{\dot{M}_w} - 1\right), \tag{4}$$

where $\dot{M}_w$ is the wind mass-loss rate and $\dot{M}(r) = 4\pi r^2\rho v$ is the mass flow rate at a given radius. This material should contain dust, since the injected mass is a remnant of the primordial molecular cloud material. Accordingly, the third term of equation (3) corresponds to photons absorbed by the dust in the flow material that comes from the evaporating globules. The first term corresponds to the ionizing photons absorbed by evaporation of the globules, and the second term corresponds to the photons absorbed by newly recombined gas.

The absorption of photons by dust and by hydrogen atoms produced by recombinations reduces the flux of ionizing photons that arrives at the surface of a globule, F_g, and therefore it reduces the hydrogen nucleus flux injected by the photoevaporation of each globule given by $n_{i0}\,c_i = F_g$, where n_{i0} is the density at the D-critical type ionization front (IF) moving slowly into the globule. This condition expresses the physical result that each Lyman-continuum photon that reaches the surface of the globule liberates an electron/proton pair. The assumption of a D-critical type ionization front implies that the injection velocity of the photoevaporated material in equation (2) is $v_{\rm inj} = c_i$.

In the absence of dust, the flux of ionizing photons that arrives at the surface of a photoevaporated globule is given by

$$F_g = F - \int_{R_g}^{\infty}\alpha_R n_i^2\,dl\,, \tag{5}$$

where $F = \dot{S}/4\pi r^2$ is the flux of ionizing photons from the star, and l is the distance to the center of the globule. Taking the density profile of the photoevaporating globule as $n_i = n_{i0}(l/R_g)^{-2}$ (see Dyson 1968 for an exact solution), the above equation becomes a quadratic equation for n_{i0}, given F (Spitzer 1978). Since recombinations in the dense evaporating flow of the globule dominate, F is approximately equal to the columnar recombination rate. Then

$$n_{i0} = \left(\frac{3\dot{S}}{4\pi\alpha_R R_g r^2}\right)^{1/2} \simeq 3 \times 10^5 \dot{S}_{49}^{1/2} R_{g16}^{-1/2} r_{17}^{-1}\ {\rm cm}^{-3}\,, \tag{6}$$

where $R_{g16} = R_g/10^{16}$ cm, $r_{17} = r/10^{17}$ cm, and $\dot{S}_{49} = \dot{S}/10^{49}$ s^{-1}.

Pastor et al. (1991), using Dyson's density profile (instead of $n_i \propto l^{-2}$ assumed above), found that the effect of dust in the photoevaporation of globules in equation (5) can be parameterized as

$$F = n_{i0}\,c_i\,e^{0.45\tau_g} + 0.12\alpha_R n_{i0}^2 R_g\,e^{0.37\tau_g}\,, \tag{7}$$

where the dust opacity from infinity up to the globule surface is $\tau_g = \sigma_d n_{i0} R_g$.[4] This is a transcendental equation for n_{i0}, which is reduced with respect to the dust-free case (equation [6]). We used this equation to obtain n_{i0} and the mass source term given by

$$\dot{q} = n_{i0}\,c_i\,A_g N_g m_{\rm H}\,. \tag{8}$$

The above equations can be expressed in nondimensional variables writing r in units of the mean free path for a

[4] This equation is valid for $\tau_g < 10$, which is always true for our models.

photon to hit a globule $r_0 = (A_{g0} N_g)^{-1}$, where $A_{g0} = \pi R_{g0}^2$ is the initial globule area at $t = 0$ (see § 2.3); v in units of c_i; the photon rate normalized as $\dot{s} = \dot{S}/\dot{S}_*$, where $\dot{S}_*$ is the stellar photon rate; ρ in units of $\rho_0 = m_{\rm H}(\dot{S}_*/4\pi r_0^3 \alpha_R)^{1/2}$, hence, the number density in units of $n_0 = \rho_0/m_{\rm H}$; the mass flux normalized as $\dot{m} = \dot{M}/\dot{M}_0$, where $\dot{M}_0 = 4\pi r_0^2 \rho_0 c_i$; and the mass source term $\dot{q}$ in units of $\dot{q}_0 = n_0 c_i A_{g0} N_g m_{\rm H}$. The parameter r_0 is approximately the Strömgren radius of the mass-loaded wind; ρ_0, $\dot{M}_0$, and $\dot{q}$ are the corresponding parameters evaluated at r_0. This can be seen by equating the mass flow through the Strömgren surface to the total mass-loading rate of all the globules inside of r_0. It is interesting to note that in this case of Lyman-induced, photoevaporative mass loaded winds, r_0 is independent of $\dot{S}_*$, and the Strömgren radius of the models is not very sensitive to $\dot{S}_*$ (see, e.g., Table 2). Increasing $\dot{S}_*$ increases the photoevaporative rate, which increases the density in the wind, which thereby keeps the Strömgren radius constant. We note also that the mean separation between globules, l_g, is of order $N_g^{-1/3}$, and that the Strömgren radius is of order $l_g(l_g/R_{g0})^2$.

Furthermore, to take into account the reduced mass injection in the central zone of the H II region as the area of the photoevaporating globules, A_g, decreases with time, a function $g(r, t)$ is introduced, such that $A_g = A_{g0}\, g(r, t)$ (see § 2.3). Equations (1)–(3) can be written in terms of the nondimensional variables as

$$\frac{d\dot{m}}{dr} = r^2 n_{i0}\, g\,, \tag{9}$$

$$\frac{dv^2}{dr} = \frac{2v^2[r^3 n_{i0}\, g(1 + v + v^2) - 2\dot{m}]}{\dot{m} r(1 - v^2)}\,, \tag{10}$$

where the normalized velocity of the injected material is set $v_{\rm inj} = 1$, since a D-critical IF was assumed; and

$$\frac{d\dot{s}}{dr} = -\dot{s} g - \left(\frac{\dot{m}}{rv}\right)^2 - \tau_0\, n_{\rm inj}\, \dot{s}\,, \tag{11}$$

where $\tau_0 = \sigma_d n_0 r_0$, and the nondimensional mass injected by the photoevaporating globules is

$$n_{\rm inj} = \frac{\dot{m}_w}{r^2 v}\left(\frac{\dot{m}}{\dot{m}_w} - 1\right), \tag{12}$$

where $\dot{m}_w$ is the nondimensional wind mass-loss rate. The density in the globule ionization front is obtained from the nondimensional equation (7),

$$\frac{\dot{s}}{r^2} = \beta n_{i0}^2\, g^{1/2} e^{0.37\tau_{g0} n_{i0} g^{1/2}} + \epsilon n_{i0}\, e^{0.45\tau_{g0} n_{i0} g^{1/2}}\,, \tag{13}$$

where $\beta = 0.12 R_{g0}/r_0$, and $\epsilon = (4\pi r_0/\alpha_R \dot{S}_*)^{1/2} c_i$, and the globule optical depth is $\tau_{g0} = \tau_0 R_{g0}/r_0$.

Equations (9)–(11) can be solved given the boundary conditions at the stellar radius: $\dot{s}(r_*) = 1$, $\dot{m}(r_*) = \dot{M}_w/\dot{M}_0$, $v(r_*) = v_w/c_i$, where v_w is the wind velocity. Note that equation (10) has a critical point when $3r^3 n_{i0}\, g = 2\dot{m}$. This critical point depends on the nondimensional photon rate $\dot{s}$ through equation (13) and, as will be shown in § 3, flow solutions go through a shock and through a sonic point at this critical point. This sonic transition occurs when the rate of ionizing photons decreases, i.e., one can show that there is no sonic point if $\dot{s} = 1$. Our result is consistent with the sonic transition discussed by Williams, Hartquist, & Dyson (1994) for mass-loaded barotropic flows (see also Hartquist et al. 1986). They considered a uniform mass-loading term such that the sonic transition occurs at the edge of the mass-loading region at which the gradients in the flow variables become infinite. In our case, if $\tau_0 = 0$ the mass loading decreases, as the square root of the flux of ionizing photons, $\dot{q} \propto (\dot{s}/r^2)^{1/2}$, which decreases continuously with distance from the central star. The sonic transition occurs in the region in which $\dot{s}$ decreases abruptly to 0.

To fix the normalization, we will take as reference values $R_{g0} = 0.01$ pc and a number density of $N_g = 2 \times 10^4$ pc^{-3} (see discussion in § 2.1). In terms of these reference values, the normalization units can be written as

$$\left(\frac{r_0}{\rm pc}\right) = 1.6 \times 10^{-1}\left(\frac{R_{g0}}{0.01\ {\rm pc}}\right)^{-2}\left(\frac{N_g}{2 \times 10^4\ {\rm pc}^{-3}}\right)^{-1}, \tag{14a}$$

$$\left(\frac{n_0}{\rm cm^{-3}}\right) = 5.7 \times 10^3\left(\frac{R_{g0}}{0.01\ {\rm pc}}\right)^{3}\left(\frac{N_g}{2 \times 10^4\ {\rm pc}^{-3}}\right)^{3/2} \times \left(\frac{\dot{S}_*}{10^{49}\ {\rm s}^{-1}}\right)^{1/2}, \tag{14b}$$

$$\left(\frac{\dot{M}_0}{M_\odot\ {\rm yr}^{-1}}\right) = 4.5 \times 10^{-4}\left(\frac{R_{g0}}{0.01\ {\rm pc}}\right)^{-1}\left(\frac{N_g}{2 \times 10^4\ {\rm pc}^{-3}}\right)^{-1/2} \times \left(\frac{\dot{S}_*}{10^{49}\ {\rm s}^{-1}}\right)^{1/2}, \tag{14c}$$

and

$$\tau_0 = 5.6\left(\frac{R_{g0}}{0.01\ {\rm pc}}\right)\left(\frac{N_g}{2 \times 10^4\ {\rm pc}^{-3}}\right)^{1/2}\left(\frac{\dot{S}_*}{10^{49}\ {\rm s}^{-1}}\right)^{1/2}. \tag{14d}$$

2.3. *Evolution of Photoevaporated Neutral Globules*

To study the effect of the photoevaporation on the globules, we consider a simple model such that the mass M_g and radius R_g of a globule at a time t is related to its mass M_{g0} and radius R_{g0} at $t = 0$ by $M_g(t)/R_g(t) = M_{g0}/R_{g0}$ (valid, e.g., if the globules are virialized and evolve with a constant velocity dispersion). For simplicity, we ignore the attenuation of ionizing photons, i.e., $\dot{s}(r) = 1$. This assumption overestimates the destruction of the globules close to the Strömgren radius at which $\dot{s} \to 0$.

The evolution of the globule's mass at a fixed distance from the star r is given by

$$\frac{\partial M_g}{\partial t} = -n_{i0}\, c_i\, A_g\, m_{\rm H}\,. \tag{15}$$

With the above assumptions, this equation can be rewritten in nondimensional variables and in terms of the area function $g(r, t)$, such that $R_g = R_{g0}\, g(r, t)^{1/2}$ as

$$\frac{\partial g}{\partial t} = -n_{i0}\, g^{3/2}\,, \tag{16}$$

where the time has been normalized with $t_0 = M_{g0}(2n_0 c_i A_{g0} m_{\rm H})^{-1}$. In the dust-free case (equation [13], with $\tau_0 = 0$ and $\epsilon = 0$), this equation can be integrated analytically, giving

$$g_{\rm nd}(r, t) = 1\Big/\left(1 + \frac{1}{4\beta^{0.5}}\frac{t}{r}\right)^4, \tag{17}$$

where the subscript "nd" refers to "no dust." This equation shows that the evaporation of globules is more efficient in the center, in which the photon flux is higher. This equation implies that, if all the globules inside the H II region are identical at $t = 0$, then, at a later time t, there is a "destruction radius" $r_d \equiv (t/4)\beta^{-0.5}$ that corresponds to the distance from the star inside which the globules' radius have decreased by a factor of 4. The numerical value of this destruction radius is

$$\left(\frac{R_d}{\mathrm{pc}}\right) = 0.02\left(\frac{M_{g0}}{1\ M_\odot}\right)^{-1}\left(\frac{\dot{S}_*}{10^{49}\ \mathrm{s}^{-1}}\right)^{1/2} \times \left(\frac{R_{g0}}{0.01\ \mathrm{pc}}\right)^{3/2}\left(\frac{t}{5\times 10^4\ \mathrm{yr}}\right).$$

Including the effect of dust, equation (16) can be integrated numerically, given the transcendental equation for n_{i0} (eq. [13]). The evolution of standard globules exposed to the radiation field of an O6 star is presented in Figure 2, which shows $g(r, t)$ as a function of nondimensional distance to the central star for different times: $t_3 = 10^3$, $t_4 = 10^4$, and $t_5 = 10^5$ yr, where t measures the time since the evaporation of the globules began. The continuous lines correspond to the evolution of dusty globules, and the dashed lines correspond to the evolution of dust-free globules for the same times. This figure shows that the effect of the dust is very important in the survival of the globules: the ionizing photons are absorbed by dust in the evaporating flows of the globules, and the dusty globules survive for longer times.

Figure 3 shows the nondimensional mass source function $\dot{q}/\dot{q}_0$ for the dusty globules as a function of nondimensional distance to the central star. The continuous lines correspond to models with dust at times $t_3 = 10^3$, $t_4 = 10^4$, and $t_5 = 10^5$ yr from top to bottom. The dashed lines correspond to dust-free models for the same times. This figure shows the effect of dust in the evolution of $\dot{q}$ and therefore on the evolution of the mass-loaded ionized winds. Dust lowers the mass injection rate because of its attenuation effect on the photoevaporating photons.

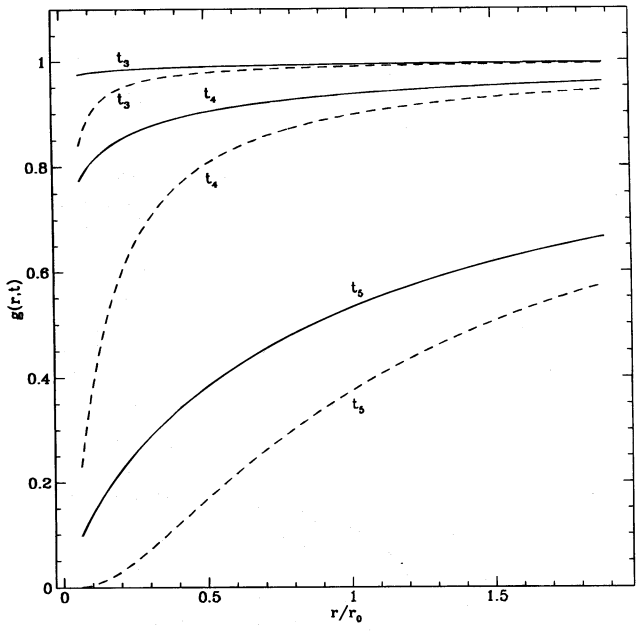

FIG. 2.—The function $g(r, t)$ as a function of nondimensional distance to the central star for different times: $t_3 = 10^3$, $t_4 = 10^4$, and $t_5 = 10^5$ yr. Continuous lines correspond to the evolution of dusty globules, and dashed lines correspond to the evolution of dust-free globules for the same times.

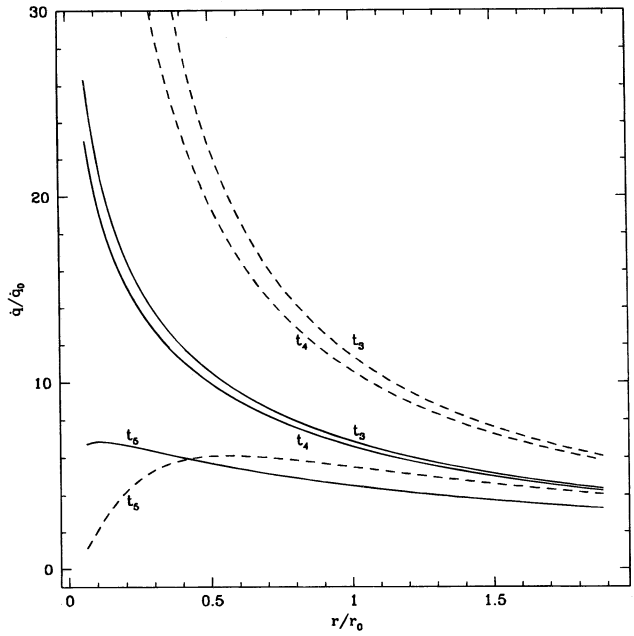

FIG. 3.—The nondimensional mass source function $\dot{q}/\dot{q}_0$ for the dusty globules as a function of nondimensional distance to the central star. Continuous lines correspond to models with dust at times $t_3 = 10^3$, $t_4 = 10^4$, and $t_5 = 10^5$ yr from top to bottom. Dashed lines correspond to dust-free models for the same times.

Hence, the function $g(r, t)$ takes into account the evolution (shrinking) of the globules due to photoevaporation. With this simple model, we take into account a reduced mass injection in the central zone of the H II region as the globules are photoevaporated.

3. RESULTS

In the models we will consider as source of winds and ionizing photons zero-age main-sequence stars of spectral types O6, O9, and B0. Their properties are shown in Table 1. These values are taken as representative of massive stars (see, e.g., Panagia 1973; Lamers & Leitherer 1993; Vilkoviskij & Tambovtseva 1992).

We consider first models of winds loaded with mass from the evaporation of standard neutral globules with $R_{g0} = 0.01$ pc, $N_g = 2 \times 10^4$ pc^{-3}, and a mass of $M_{g0} = 1\ M_\odot$. Table 2 shows the global properties of photoevaporated models for each central star evaporating standard globules: case A, O6 star; case B, O9 star; and case C, B0 star. The first column is the time since the photoevaporation of the globules began, immediately after the initial Strömgren radius is established. This time is used in the integration of equation (16) to take into account the reduced mass injec-

TABLE 1

PROPERTIES OF THE CENTRAL STARS

Star	$\dot{S}_*$ (s^{-1})	$\dot{M}_w$ ($M_\odot$ yr^{-1})	v_w (km s^{-1})
O6.....	1.2×10^{49}	1×10^{-6}	2800
O9.....	1.2×10^{48}	1×10^{-7}	2500
B0	2.3×10^{47}	6×10^{-8}	2200

TABLE 2

GLOBAL PROPERTIES OF MODELS EVAPORATING STANDARD GLOBULES

Age (yr)	r_S/r_0	$\langle n^2\rangle^{1/2}/n_0$	$\dot{M}_S/\dot{M}_0$	v_S/c_i	r_{sonic}/r_0	$\dot{S}_{sonic}/\dot{S}_*$	r_{shock}/r_0
			Case A[a]				
0.	0.49	1.84	0.29	1.18	0.465	0.0084	0.312
10^3.....	0.49	1.83	0.29	1.18	0.469	0.0084	0.315
10^4.....	0.51	1.75	0.30	1.18	0.488	0.0084	0.322
10^5.....	0.71	1.18	0.34	1.19	0.673	0.0083	0.400
			Case B[b]				
0.	0.42	2.91	0.22	1.26	0.384	0.0098	0.130
10^3.....	0.43	2.88	0.22	1.26	0.388	0.0095	0.130
10^4.....	0.44	2.78	0.22	1.25	0.401	0.0094	0.133
10^5.....	0.56	2.06	0.26	1.25	0.518	0.0088	0.160
			Case C[c]				
0.	0.42	3.82	0.28	1.29	0.377	0.0188	0.12
10^3.....	0.43	3.79	0.28	1.29	0.380	0.0184	0.12
10^4.....	0.43	3.72	0.29	1.29	0.388	0.0183	0.12
10^5.....	0.51	3.02	0.32	1.28	0.465	0.0170	0.14

[a] Central star O6: $r_0 = 1.59 \times 10^{-1}$ pc, $n_0 = 6.27 \times 10^3$ cm^{-3}, $\dot{M}_0 = 4.90 \times 10^{-4}\ M_\odot$ yr^{-1}.

[b] Central star O9: $r_0 = 1.59 \times 10^{-1}$ pc, $n_0 = 1.98 \times 10^3$ cm^{-3}, $\dot{M}_0 = 1.55 \times 10^{-4}\ M_\odot$ yr^{-1}.

[c] Central star B0: $r_0 = 1.59 \times 10^{-1}$ pc, $n_0 = 8.67 \times 10^3$ cm^{-3}, $\dot{M}_0 = 6.77 \times 10^{-5}\ M_\odot$ yr^{-1}.

tion in the center of the H II regions as the globules evaporate. The second column is the nondimensional Strömgren radius, R_S/r_0. The third column is the nondimensional root mean square density, $\langle n^2\rangle^{1/2}/n_0$, of the H II region. The fourth column is the nondimensional mass flow rate of the ionized flow at the Strömgren radius, $\dot{M}_S/\dot{M}_0$. The fifth column is the ratio of the flow speed at the Strömgren radius v_S to the sound speed c_i. The sixth, seventh, and eighth columns are the nondimensional sonic radius, ionizing photon rate, and nondimensional shock radius respectively. The last three columns are useful in obtaining the detailed numerical solutions discussed below. The normalization units are given by equations (14a)–(14b) and are indicated in each case.

Figure 4 shows the logarithm of nondimensional velocity, the logarithm of the nondimensional number density, the nondimensional ionizing photon rate, and the nondimensional mass flux as a function of the logarithm of the nondimensional distance to the central star, for model A at $t = 0$ yr. Up to $t \sim 1 \times 10^3$ yr, the solutions are almost identical because the globules have not yet been destroyed in the center and the mass loading is efficient (see global properties Table 2). This model has an isothermal shock at $r_{shock}/r_0 = 0.312$ and a sonic point at $r_{sonic}/r_0 = 0.465$. According to equations (9)and (11), the mass flow rate $\dot{m}$ is continuous through the shock, with a continuous derivative, while the photon flux is continuous but with a discontinuous derivative as shown in the figure. Figure 5 shows the same model at $t = 10^5$ yr. At this time, the model has an isothermal shock at a radius $r_{shock}/r_0 = 0.40$ and a sonic point at a radius $r_{sonic}/r_0 = 0.673$. Because the globules have been evaporated in the center, the density profile goes as $n \propto r^{-2}$ in this region (an unloaded, constant velocity, free-flowing stellar wind), until the mass loading starts and flattens the profile, trapping the ionization front of the H II region. As the globules are evaporated, the H II region becomes more extended with a smaller mean density. It is notable that although the ionized gas is flowing outward, because of the deceleration and mass loading on the flow, the electron density actually decreases with radius in the outer regions. The two solutions shown in Figures 4 and 5

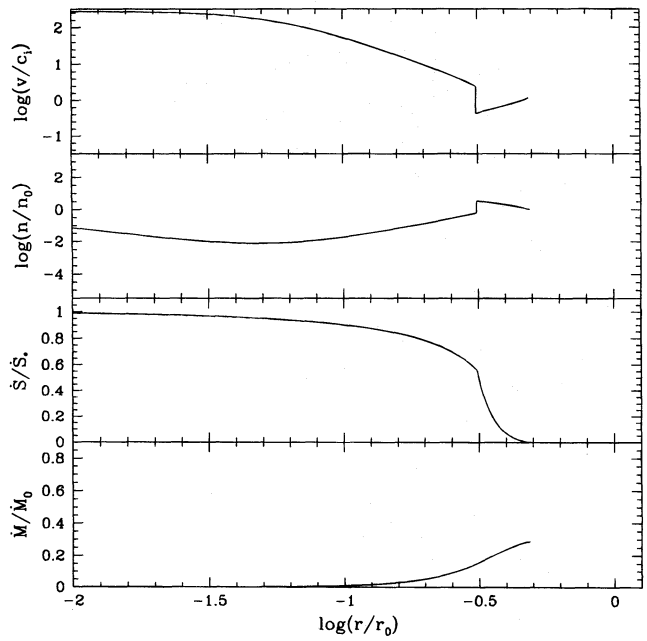

FIG. 4.—Model of an isothermal stellar wind loaded with mass injected by photoevaporating globules. The central star has an ionizing photon rate $\dot{S}_* = 1.2 \times 10^{49}$ s^{-1}, a stellar wind mass-loss rate $\dot{M}_w = 10^{-6}\ M_\odot$ yr^{-1}, and a stellar wind velocity $v_w = 2800$ km s^{-1} (see Table 2). The figure presents the logarithm of the nondimensional velocity, the logarithm of the nondimensional number density, the nondimensional ionizing photon rate, and the nondimensional mass flux as a function of the logarithm of the nondimensional distance to the central star at a time $t = 0$ yr. This model has an isothermal shock at a radius $r_{shock}/r_0 = 0.312$ and a sonic point at a radius $r_{sonic}/r_0 = 0.465$. The dimensional global properties of these models are shown in Table 2.

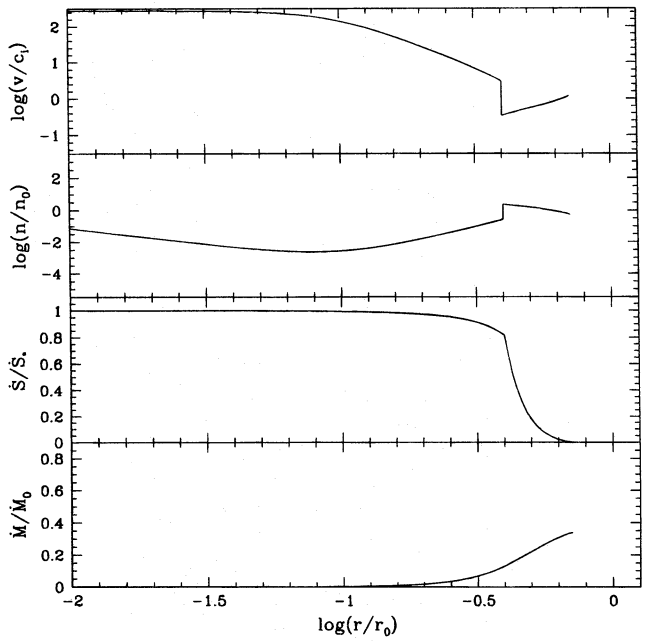

FIG. 5.—Same as Fig. 4 but for a time $t = 10^5$ yr. This model has an isothermal shock at a radius $r_{shock}/r_0 = 0.40$ and a sonic point at a radius $r_{sonic}/r_0 = 0.673$. The global properties of these models are shown in Table 2.

are representative of all the solutions in the parameter space explored: the Strömgren radius of mass-loaded H II region increases with time as the globules are evaporated in the center and the mean density decreases. Also, the shock radius and the sonic radius increase as the loading of mass decreases in the center.

Table 3 shows models for different stars at $t = 0$ yr, where the number density of the globules has been increased to $N_g = 5 \times 10^4$ pc^{-3}. Except for the first column that corresponds to the central star used in the model, the rest of the columns correspond to those described above for Table 2. An examination of Tables 2 and 3 shows that the models with higher number density of globules predict H II regions with smaller sizes and higher densities than the models with lower number density of globules.

Table 4 shows the global properties of photoevaporated models for the three different central stars evaporating standard globules without dust. At $t = 0$, these dust-free models have higher densities and smaller sizes than their dusty counterparts in Table 2. These models evolve faster than the models with dust, and at $t = 10^5$ yr they have similar sizes although higher densities.

Finally, Table 5 shows the effect of changing the stellar mass-loss rate for a central star with $\dot{S}_* = 1.2 \times 10^{49}$ s^{-1} and a stellar wind velocity $v_w = 2800$ km s^{-1}, evaporating standard globules. This table shows that the major effect of

TABLE 3

GLOBAL PROPERTIES OF MODELS EVAPORATING GLOBULES WITH $N_g = 5 \times 10^4$ pc^{-3} AND $R_{g0} = 0.01$ pc ($t = 0$ yr)

Star	r_S/r_0	$\langle n^2\rangle^{1/2}/n_0$	$\dot{M}_S/\dot{M}_0$	v_S/c_i	r_{sonic}/r_0	$\dot{S}_{sonic}/\dot{S}_*$	r_{shock}/r_0
O6[a]	0.77	0.82	0.40	1.14	0.75	0.0065	0.575
O9[b]	0.60	1.57	0.26	1.22	0.56	0.0078	0.238
B0[c]	0.59	2.14	0.33	1.25	0.54	0.0140	0.208

[a] Central star O6: $r_0 = 6.37 \times 10^{-2}$ pc, $n_0 = 2.48 \times 10^4$ cm^{-3}, $\dot{M}_0 = 3.10 \times 10^{-4}$ $M_\odot$ yr^{-1}.
[b] Central star O9: $r_0 = 6.37 \times 10^{-2}$ pc, $n_0 = 7.84 \times 10^3$ cm^{-3}, $\dot{M}_0 = 9.81 \times 10^{-5}$ $M_\odot$ yr^{-1}.
[c] Central star B0: $r_0 = 6.37 \times 10^{-2}$ pc, $n_0 = 3.43 \times 10^3$ cm^{-3}, $\dot{M}_0 = 4.28 \times 10^{-5}$ $M_\odot$ yr^{-1}.

TABLE 4

GLOBAL PROPERTIES OF MODELS EVAPORATING STANDARD GLOBULES: NO DUST

Age (yr)	r_S/r_0	$\langle n^2\rangle^{1/2}/n_0$	$\dot{M}_S/\dot{M}_0$	v_S/c_i	r_{sonic}/r_0	$\dot{S}_{sonic}/\dot{S}_*$	r_{shock}/r_0
			Case A[a]				
0.	0.39	6.32	0.46	1.24	0.355	0.0415	0.155
10^5	0.67	3.00	0.60	1.19	0.638	0.0260	0.255
			Case B[b]				
0.	0.39	6.53	0.38	1.26	0.347	0.0340	0.075
10^5	0.54	4.14	0.47	1.22	0.505	0.0250	0.115
			Case C[c]				
0.	0.39	6.32	0.39	1.29	0.350	0.0386	0.084
10^5	0.49	4.70	0.44	1.26	0.451	0.0306	0.105

[a] Central star O6: $r_0 = 1.59 \times 10^{-1}$ pc, $n_0 = 6.27 \times 10^5$ cm^{-3}, $\dot{M}_0 = 4.90 \times 10^{-4}$ $M_\odot$ yr^{-1}.
[b] Central star O9: $r_0 = 1.59 \times 10^{-1}$ pc, $n_0 = 1.98 \times 10^3$ cm^{-3}, $\dot{M}_0 = 1.55 \times 10^{-4}$ $M_\odot$ yr^{-1}.
[c] Central star B0: $r_0 = 1.59 \times 10^{-1}$ pc, $n_0 = 8.67 \times 10^3$ cm^{-3}, $\dot{M}_0 = 6.77 \times 10^{-5}$ $M_\odot$ yr^{-1}.

TABLE 5

GLOBAL PROPERTIES OF MODELS EVAPORATING STANDARD GLOBULES: CHANGE OF $\dot{M}_w$

$\dot{M}_w$ ($M_\odot$ yr^{-1})	r_S/r_0	$\langle n^2\rangle^{1/2}/n_0$	$\dot{M}_S/\dot{M}_0$	v_S/c_i	r_{sonic}/r_0	$\dot{S}_{sonic}/\dot{S}_*$	r_{shock}/r_0
Central Star O6[a]: $\dot{S}_* = 1.2 \times 10^{49}$; $v_w = 2800$ km s^{-1}							
10^{-8}	0.42	1.13	0.07	1.25	0.384	0.0011	0.038
10^{-7}	0.43	1.47	0.11	1.24	0.390	0.0021	0.103
10^{-6}	0.49	1.84	0.29	1.18	0.465	0.0084	0.312
10^{-5}	1.00	6.00	1.70	2.18	...	...	...

[a] $r_0 = 1.59 \times 10^{-1}$ pc, $n_0 = 6.27 \times 10^3$ cm^{-3}, $\dot{M}_0 = 4.90 \times 10^{-4}\ M_\odot$ yr^{-1}.

changing $\dot{M}_w$ is that the position of the shock moves inward as the mass-loss rate decreases. It shows also that for a high enough wind mass-loss rate (e.g., $\dot{M}_w = 10^{-5}\ M_\odot$ yr^{-1}) it is possible to obtain solutions without shocks, where the ionized flow is decelerated smoothly as it is mass loaded but is always supersonic.

4. DISCUSSION

Figure 6 plots the root mean square densities versus the ionized "Strömgrem" diameters derived for the different models presented here. The three lines connecting the filled triangles represent the mean densities versus radii as a function of time predicted by models using standard globules and for three different central stars (O6, O9, and B0, from top to bottom, respectively). The first point in each line corresponds to $t = 0$ yr, and the last point corresponds to $t = 10^5$ yr (see Table 2). If globules with lower (higher) masses are considered, the times can be simply scaled changing t_0. The same figure shows as isolated filled squares the models in Table 3 with $N_g = 5 \times 10^4$ pc^{-3} (from top to bottom, the central star is O6, O9, and B0). This figure shows that stellar winds mass loaded by the photoevaporation of PIGs can survive as compact H II regions for times $t \gtrsim 10^5$ yr, depending on the properties of the PIGs. Note that the H II regions evolve faster as the inner globules are destroyed. Furthermore, survival timescales much longer than 10^5 yr would require a high number density of globules with masses much larger than 1 $M_\odot$, which would be difficult to justify observationally. Also, models without dust are shown with filled circles connected with a dashed line, corresponding to $t = 0$ yr and $t = 10^5$ yr, respectively. From top to bottom they correspond to an O6, O9, and B0 central star, respectively (see Table 4). These models evolve faster because the dust-free globules are evaporated faster than the dusty globules. The isolated filled square in the upper left corner corresponds to the extreme case of an O6 star evaporating globules with $N_g = 5 \times 10^6$ pc^{-3}, $R_{g0} = 0.001$ pc; the isolated filled square in the lower right corner corresponds to the case of an O6 star evaporating protoplanetary disks with $N_g = 3 \times 10^4$ pc^{-3}, $R_{g0} = 0.001$ pc (see below). These evaporating disks would correspond to the "proplyds" discovered by O'Dell, Wen, & Hu (1993) and O'Dell & Wen (1994).

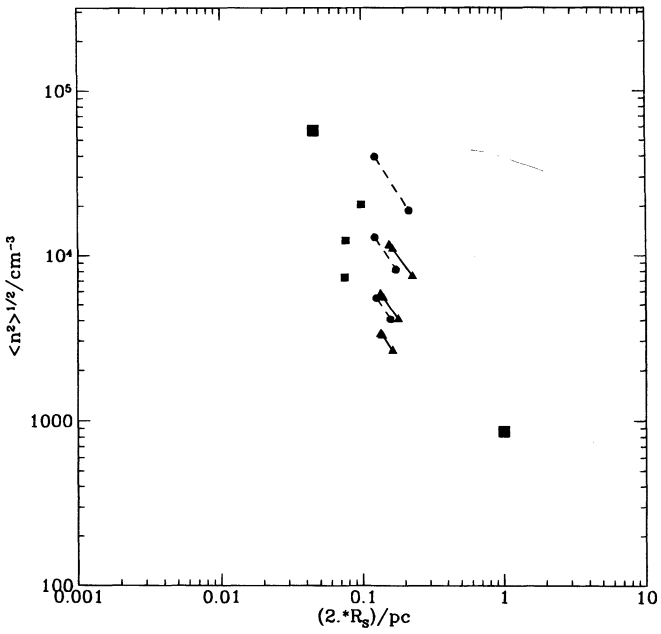

FIG. 6.—The root mean square densities vs. the ionized "Strömgren" diameters for the different models in this work. The three lines connecting the filled triangles represent the mean densities vs. radii as a function of time predicted by models using standard globules and for the three different central stars (O6, O9, and B0, from top to bottom, respectively). The first point in each line corresponds to $t = 0$ yr, the last point corresponds to $t = 10^5$ yr (see Table 2). The isolated filled squares are the models in Table 3 for $N_g = 5 \times 10^4$ pc^{-3} (from top to bottom, the central star is an O6, O9, and B0). The isolated filled square in the top left corner corresponds to the model of an O6 star evaporating globules with $N_g = 5 \times 10^6$ pc^{-3} and $R_{g0} = 10^{-3}$ pc. The isolated filled square in the bottom right corner corresponds to a model of an O6 star evaporating globules with $N_g = 3 \times 10^4$ pc^{-3} and $R_{g0} = 10^{-3}$ pc. Models without dust (Table 4) are shown with filled circles that correspond to $t = 0$ yr and $t = 10^5$ yr, respectively.

A change in the properties of the globules will result in models with different mean densities and radii. Recall that our standard model has $R_{g0} = 0.01$ pc and $N_g = 2 \times 10^4$ pc^{-3}. As shown in Table 3, if the number density of the globules N_g increases, the mean densities of the H II regions increase, and the size decrease with respect to the models in Table 2, which evaporate standard globules. On the other hand, smaller globules result in less mass loading, which decreases the flow density and increases the Strömgren radius. In particular, mass loading by protostellar disks with radii $R_g \sim 10^{-3}$ pc, number density $N_g \sim 3 \times 10^4$ pc^{-3}, and masses $M_g \sim 1 \times 10^{-2}\ M_\odot$ (McCaughrean & Stauffer 1994), produces ionized flows with low densities ($\langle n^2\rangle^{1/2} \sim 850$ cm^{-3}) and large sizes ($R_S \sim 0.5$ pc). Since they load mass very inefficiently in the wind, in this simple model they are not an important source of mass to maintain compact H II regions. An interesting possibility that may allow a more efficient mass loading for this latter type of objects is that a photodissociated flow, preceding the photoionized flow in the globule, may boost the mass loading (Hollenbach, Johnstone, & Shu 1996).

To compare the model predictions with the observed properties of compact H II regions, we plot in Figure 7 the root mean square densities versus the diameters derived for

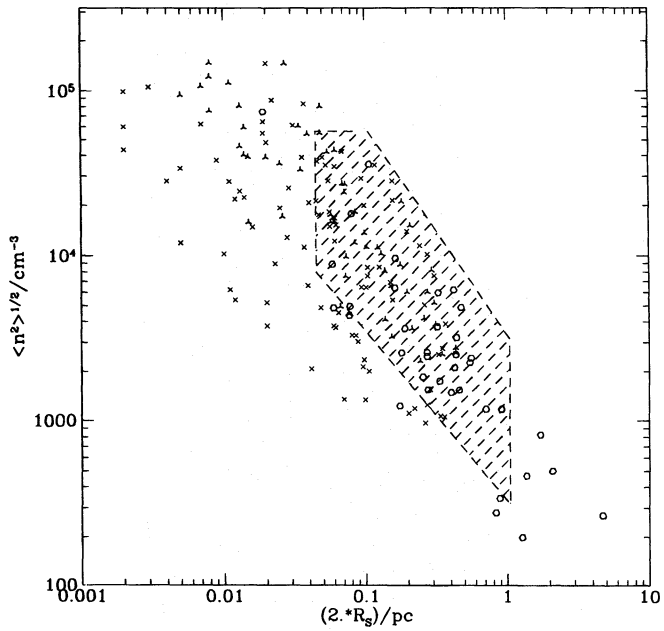

FIG. 7.—The root mean square densities vs. the diameters derived for ultra compact and compact H II regions: the surveys of WC (*open triangles*), KCW (*crosses*), and GRMC (*open hexagons*). The shaded area indicates the range of densities and sizes of the models of mass-loaded stellar winds.

ultracompact and compact H II regions. The data for ultracompact H II regions is taken from the survey of WC (*open triangles*) and from KCW (*crosses*), while that for compact H II regions is taken from GRMC (*open hexagons*). The shaded area indicates the range of densities and sizes of the models presented in this work. This figure shows that models of stellar winds from massive star mass loaded by photoevaporated globules cover a significant region of the parameter space of the compact H II regions.

It is important to point out that in our models we considered constant globule number densities N_g, since this parameter is very difficult to determine. It is interesting to consider what would happen if this density is a function of distance to the central star. In particular, if the distribution of neutral globules around the star is truncated spatially before the ionizing photons are completely absorbed, the ionization front will not be trapped. In this case, the mass-loaded wind will have its density increased in the region of mass loading plus a fast drop of the emission measure after the truncation radius, resulting in a compact H II region with a core/halo morphology for as long as the neutral globules survive. This could move the model points upward and to the left in Figures 6 and 7 and could fill in some additional parameter space in this region.

The effect of dust absorption of ionizing photons is to reduce the mass injection from the globules due to the absorption of photons by dust in the evaporating flows, and to decrease the size of the H II regions because of dust absorption of photons in the mean flow. Because of these two effects, the dusty H II regions have smaller densities than their dust-free counterparts, but similar sizes (compare Tables 2 and 4). Models with dust evolve more slowly, since the dusty globules survive for longer times than the dust-free ones.

Finally, as seen in Tables 2, 3, and 4, the velocity of the ionized gas at the Strömgren radius is quite constant in all the models, $v_S/c_i \sim 1.2$–1.3. Once the wind is mass loaded, only accelerations to thermal speeds are possible. Then, in these models the stellar winds have been decelerated to $v(r_S) \sim 16$ km s^{-1} by the mass loading, and the mass flow rates of the ionized flow have increased to $\dot{M}_S \sim 10^{-5}$ to 10^{-4} $M_\odot$ yr^{-1} at r_S, depending on the rate of ionizing photons. This ionized flow could be studied in radio recombination lines, looking for weak emission in extended wings. Recently Gaume et al. (1995) detected toward the UC H II region NGC 7538–IRS 1 emission in the H66α line with about 180 km s^{-1} widths (FWHM). They interpreted the wide emission as arising from an ionized stellar wind evaporating neutral clumps, seen in their continuum map as bright emission clumps. If we apply our model to the extreme conditions of this source, inferred from their continuum map: $N_g \sim 5 \times 10^6$ pc^{-3}, $R_{g0} = 0.001$ pc, we obtain $r_S \sim 0.02$ pc, $\langle n^2\rangle^{1/2} \sim 6 \times 10^4$ cm^{-3}, and $\dot{M} = 10^{-4}$ $M_\odot$ yr^{-1}. This model is shown as the upper left filled square in Figure 6. Although our model is very idealized,[6] it can reproduce the global properties of this source.

After r_S, these mass-loaded winds should recombine and accelerate, as the flow expands adiabatically, to a terminal velocity $v_{H\,I} \sim 40$ km s^{-1}. This velocity is obtained by considering only the adiabatic expansion of the flow, in which case $v \rightarrow v(r_S)[1 + 2\gamma/(\gamma - 1)]^{1/2}$, and using $\gamma = 5/3$. We note that this flow speed can be decreased and the neutral mass flow rate increased if there is still mass loading by hydrodynamical ablation from globules outside r_S. A detailed modeling of this neutral flow is beyond the scope of this paper. Therefore, massive neutral outflows will accompany the compact H II regions produced by the mass loading of the ionized stellar wind. These neutral flows could be observed in absorption against the continuum of the H II region. Neutral flows of this kind may also provide the origin of the fast CO outflows observed around compact and UC H II regions (Harvey & Forveille 1988; Shepard & Churchwell 1994).

5. CONCLUSIONS

Fast isothermal ionized stellar winds mass loaded by photoevaporated globules surrounding the massive stars can trap the ionization front for 10^5 yr, depending on the physical characteristics (number density, mass, and radius) of the neutral globules inside the H II region. These mass-loaded winds would then help to lengthen the compact phase of H II regions for timescales long enough to explain the large number of compact H II regions observed around O stars.

In the case of neutral globules of the characteristic sizes and observed number densities of the so-called PIGs, we find that the mean densities and sizes of the ionized regions of these mass-loaded winds correspond to those observed in compact H II regions: electron densities $n_e \sim 10^3$–10^4 cm^{-3} and diameters $D \sim 0.1$ pc. The detection of the proposed globules with the VLA, for instance in lines of ammonia, is a challenging project.

On the other hand, if globules with larger number densities and smaller sizes are found, as in the case of the source NGC 7538–IRS 1 ($N_g \sim 5 \times 10^6$ pc^{-3}, $R_{g0} \sim 10^{-3}$ pc), these types of UC H II regions ($r_S \sim 0.02$ pc) could also be explained as ionized mass-loaded winds, since our models

[6] As discussed by Gaume et al, this source could also have a photoevaprated disk.

can reproduce the exceedingly small sizes and high densities characteristic of these regions. Nevertheless, our models should be more appropriate to the more extended, irregular, multiple-peaked, compact H II regions detected in the radio continuum surveys. The multiple peaks would then correspond to the ionized surface of PIGs. The observed irregular regions have overall sizes similar to those of the mass-loaded wind regions presented here (see Fig. 6), while the observed continuum peaks have sizes and number densities similar to those of the standard PIGs used in our models.

The photoevaporated material should contain dust, since the neutral globules are probably remnants of primordial molecular cloud material. The effect of dust absorption of ionizing photons is to decrease the size of an H II region with a fixed electron density distribution. However, dust also reduces the mass injection rate from the globules lowering the electron density in the mass-loaded flow, which has the opposing effect of increasing the size of the H II region. The net effect is that the dusty H II regions have smaller densities than their dust free counterparts, but similar sizes. Dust also increases the survival times of the dusty neutral globules, and therefore the dusty mass-loaded winds evolve more slowly than the dust-free ones.

These models imply that this type of H II region should have ionized flows with mass flow rates of $\dot{M} \sim 10^{-5}$ to $10^{-4}\ M_{\odot}\ \mathrm{yr}^{-1}$ at r_S, depending on the rate of ionizing photons of the central star. The ionized flows could be studied in radio recombination lines. Furthermore, beyond the H II region, a neutral flow should be observed, since the ionized flow will recombine after r_S and accelerate adiabatically to a terminal velocity of $v_{\mathrm{H\,I}} \sim 40\ \mathrm{km\ s}^{-1}$. These neutral flows could be looked for at 21 cm in absorption against the continuum of the compact H II regions. These neutral flows may provide the origin of the fast CO outflows observed around compact and UC H II regions.

J. C. and S. L. acknowledge support from the grant UNAM DGAPA No. IN100793 and CONACYT No. 4916-E9406. G. G. gratefully acknowledges support from a Guggenheim Fellowship, the FONDECYT project no. 1950524, and the warm hospitality at the IA, UNAM. D. H. acknowledges support from NASA RTOP 399-20-10, which funds the Center for Star Formation Studies, a consortium of theorists from NASA Ames, UC Berkeley, and UC Santa Cruz. We thank A. Noriega and A. Königl for useful comments and suggestions. We also thank an anonymous referee for helpful comments.

REFERENCES

Arthur, S. J., & Lizano, S. 1996, in preparation
Bedjin, P. J., & Tenorio-Tagle, G. 1984, A&A, 135, 81
Bertoldi, F. 1989, ApJ, 346, 735
Bertoldi, F., & McKee, C. F. 1990, ApJ, 354, 529
Cesaroni, R., Churchwell, E., Hofner, P., Walmsley, C. M., & Kurtz, S. 1994, A&A, 288, 903
Cesaroni, R., Walmsley, C. M., & Churchwell, E. 1992, A&A, 256, 618
Churchwell, E. 1990, A&A Rev., 2, 79
Churchwell, E., Felli, M., Wood, D. O. S., & Massi, M. 1987, ApJ, 321, 516
DePree, C. G., Rodríguez, L. F., & Goss, W. M. 1995, Rev. Mexicana Astron. Astrofis., 31, 39
Dyson, J. E. 1968, Ap&SS, 1, 388
———. 1973, A&A, 27, 459
———. 1994, in Lecture Notes in Physics, Vol. 431, Star Formation Techniques in Infrared and mm-wave Astronomy, ed. T. P. Ray & S. V. W. Beckwith (Berlin: Springer-Verlag), 93
Dyson, J. E., & Williams, D. A. 1980, The Physics of the Interstellar Medium (Manchester: Manchester Univ. Press)
Dyson, J. E., Williams, R. J. R., & Redman, M. P. 1995, MNRAS, 277, 700
Felli, M., Churchwell, E., Wilson, T. L., & Taylor, G. B. 1993, A&AS, 98, 137
Felli, M., Hjellming, R. M., & Cesaroni, R. 1987, A&A, 182, 313
Franco, J., Tenorio-Tagle, G., & Bodenheimer, P. 1989, Rev. Mexicana Astron. Astrofis., 18, 65
Franco, J., Tenorio-Tagle, G., & Bodenheimer, P. 1990, ApJ, 349, 126
Garay, G. 1987, Rev. Mexicana Astron. Astrofis, 14, 489
Garay, G., Lizano, S., & Gómez, Y. 1994, ApJ, 429, 268
Garay, G., Moran, J. M., & Reid, M. J. 1987, ApJ, 314, 535
Garay, G., Moran, J. M., & Rodríguez, L. F. 1993, ApJ, 413, 582
Garay, G., & Rodríguez, L. F. 1990, ApJ, 362, 191
Garay, G., Rodríguez, L. F., Moran, J. M., & Churchwell, E. 1993, ApJ, 418, 368 (GRMC)
Gaume, R. A., Goss, W. M., Dickel, H. R., Wilson, T. L., & Johnson, K. J. 1995, ApJ, 438, 776
Hartquist, T. W., Dyson, J. E., Pettini, M., & Smith, L. 1986, MNRAS, 221, 715
Harvey, P. M., & Forveille, T. 1988, A&A, 197, L19
Hofner, P., Kurtz, S., Churchwell, E., Walmsley, C. M., & Cesaroni, R. 1996, ApJ, 460, 359
Hollenbach, D., Johnstone, D., Lizano, S., & Shu, F. H. 1994, ApJ, 428, 654
Hollenbach, D., Johnstone, D., & Shu, F. H. 1996, in preparation
Kahn, F. D. 1969, Physica, 41, 172
Kurtz, S., Churchwell, E., & Wood, D. O. S. W. 1994, ApJS, 91, 659 (KCW)
Lacques, P., & Vidal, J. L. 1979, A&A, 73, 97
Lamers, H. J. L. M., & Leitherer, C. 1993, ApJ, 412, 771
Mac Low, M., Van Buren, D., Wood, D. O. S., & Churchwell, E. 1991, ApJ, 369, 395
McCaughrean, M. J., & Stauffer, J. R. 1994, AJ, 108, 1382
O'Dell, C. R., & Wen, Z. 1994, ApJ, 436, 194
O'Dell, C. R., Wen, Z., & Hu, X. 1993, ApJ, 410, 696
Olmi, L., Cesaroni, R., & Walmsley, C. M. 1993, A&A, 276, 489
Oort, J. H., & Spitzer, L., Jr. 1955, ApJ, 121, 6
Panagia, N. 1973, AJ, 9, 929
Pastor, J., Cantó, J., & Rodríguez, L. F. 1991, A&A, 246, 551
Planesas, P., Martín-Pintado, J., & Serabyn, E. 1992, ApJ, 386, L23
Redman, M. P., Williams, R. J. R., & Dyson, J. E. 1996, MNRAS, in press
Rodríguez, L. F., & Bastian, T. S. 1994, ApJ, 428, 324
Shepard, D. S., & Churchwell, E. B. 1994, BAAS, 26, 907
Spitzer, L., Jr. 1978, Physical Processes in the Interstellar Medium (New York: Wiley)
Tenorio-Tagle, G. 1977, A&A, 54, 517
———. 1979, A&A, 71, 59
Thum, C., Martín-Pintado, J., & Bachiller, R. 1992, A&A, 256, 507
Van Buren, D., MacLow, M., Wood, D. O. S., & Churchwell, E. 1990, ApJ, 353, 570
Vilkoviskij, E. Ya., & Tambovtseva, L. V. 1992, A&AS, 94, 109
Weaver, R., McCray, R., Castor, J., Shapiro, P., & Moore, R. 1977, ApJ, 218, 377
Williams, R. J. R., Hartquist, T. W., & Dyson, J. E. 1994, ApJ, 446, 759
Wood, D. O. S. W., & Churchwell, E. 1989, ApJS, 69, 831 (WC)
———. 1991, ApJ, 372, 199
Yorke, H. W., Tenorio-Tagle, G., & Bodenheimer, P. 1983, A&A, 127, 313